Global and Planetary Change 204 (2021) 103582

Contents lists available at ScienceDirect

Global and Planetary Change

journal homepage: www.elsevier.com/locate/gloplacha

Surface hydrographic changes at the western flank of the Sicily Channel associated with the last sapropel

Sergio Trias-Navarro [a,b,*], Isabel Cacho [b], Maria de la Fuente [b], Leopoldo D. Pena [b], Jaime Frigola [b], Fabrizio Lirer [c], Antonio Caruso [a]

[a] Dipartimento di Scienze della Terra e del Mare, Università degli studi di Palermo, via Archirafi 20-22, 90123 Palermo, Italy
[b] GRC Geociències Marines, Departament de Dinàmica de la Terra i de l'Oceà, Facultat de Ciències de la Terra, Universitat de Barcelona, Campus de Pedralbes, C/Martí i Franquès s/n, 08028 Barcelona, Spain
[c] Istituto di Scienze Marine (ISMAR) – CNR, Sede Napoli, Calata Porta di Massa, Interno Porto di Napoli, 80133, Napoli, Italy

ARTICLE INFO

Editor: Dr. Fabienne Marret-Davies

Keywords:
Sapropel
Planktic foraminifera
Surface hydrography
Strait of Sicily

ABSTRACT

In the eastern Mediterranean Sea, the early Holocene was characterized by major climatic and oceanographic changes that led to the formation of the last sapropel (S1) between 10.8 and 6.1 kyr cal. BP. These hydrographic changes might have altered the water exchange between the eastern and western Mediterranean sub-basins through the Strait of Sicily, but the existing evidences are inconclusive. In the present study we show new evidence from sediment core NDT-6-2016 located at the western flank of the Sicily channel, a key location to monitor the surface/intermediate water exchange between the two Mediterranean sub-basins. We perform paleohydrographic reconstructions based on planktic foraminifera ecology for the last 15 kyr cal. BP, including the S1 deposition interval. In addition, $\delta^{18}O$ measurements in both *Globigerina bulloides* and *Globigerinoides ruber* and also major elements analyses in bulk sediment are presented. Our results show that significant changes in surface water properties occurred in W-Sicily characterized by a strong contrast in the seasonal hydrographic conditions during the S1 interval. This study proposes that the oceanographic changes in the eastern Mediterranean associated with the surface freshening promoted by the African monsoon likely triggered a restricted water exchange through the Strait of Sicily. This situation led to limited influence of the surface Atlantic waters into the studied area that favored the development of intense summer stratification and vertical winter mixing. This situation changed at about 7 kyr cal. BP when a decrease in the summer stratification probably reflected the influence of the eastward path of the surface Atlantic Waters. This situation would suggest a reinforcement of the water exchange through the Strait of Sicily that marked the end of the extreme conditions that prevailed in the eastern Mediterranean during the S1 formation.

1. Introduction

The Mediterranean Sea is a semi-enclosed sea formed by two sub-basins, the eastern Mediterranean (*E*-Med) and the western Mediterranean (W-Med), connected through the Strait of Sicily. Their physiographic characteristics make both of these sub-basins very sensitive to climatic variability as demonstrated by many paleoclimatic and paleoceanographic studies (Abrantes et al., 2012; Cacho et al., 2001; Mayewski et al., 2004; Rohling et al., 2015). An interesting phenomenon that attests this enhanced sensitivity in the *E*-Med corresponds to a series of rhythmic deep water anoxic-events that resulted in the deposition of high-organic carbon sedimentary layers, i.e. the so-called "Sapropel" events (Grant et al., 2016; Lourens et al., 1992; Murat, 1999; Rohling, 1994; Rohling et al., 2015; Rossignol-Strick, 1985; Toucanne et al., 2015).

Sapropel events occurred as a consequence of major changes in the hydrological cycle associated with stronger runoff of north African river systems into the Mediterranean Sea due to a maximum in the northern hemisphere summer insolation and monsoon intensification. The rapid influx of fresh-water promoted a strong surface ocean stratification that led to the establishment of deep-basin anoxic conditions in parallel with an increased export productivity, which resulted in the formation of sapropel layers observed in the sedimentary record (Bianchi et al., 2006; De Lange et al., 2008; Grant et al., 2016; Grimm et al., 2015; Incarbona

* Corresponding author at: Dipartimento di Scienze della Terra e del Mare, Università degli studi di Palermo, via Archirafi 20-22, 90123 Palermo, Italy.
E-mail address: sergio.trias@unipa.it (S. Trias-Navarro).

https://doi.org/10.1016/j.gloplacha.2021.103582
Received 1 October 2020; Received in revised form 5 July 2021; Accepted 14 July 2021
Available online 17 July 2021

et al., 2011; Marino et al., 2009; Rohling, 1994; Rohling et al., 2015; Rossignol-Strick, 1985; Toucanne et al., 2015). The last sapropel (S1) took place during the Holocene between ~10.8 and ~ 6.1 kyr cal. BP in the *E*-Med (De Lange et al., 2008). Several studies have focused on the detailed analysis of the oceanographic conditions associated with the S1 formation in the E-Med (Bianchi et al., 2006; Checa et al., 2020; Filippidi et al., 2016; Grimm et al., 2015; Mercone et al., 2001; Tachikawa et al., 2015; Tesi et al., 2017; Wu et al., 2017). However, only a few studies have explored in detail the inter-basin connection during these episodes and its link with past climate variability (Cornuault et al., 2018; Martínez-Ruiz et al., 2003; Murat, 1999).

The large S1 change in the evaporation-precipitation balance of the E-Med and the consequent reduction in deep water convection might have ended in reduced water exchange between the two Mediterranean sub-basins (Bethoux, 1993; Murat, 1999). Despite some modeling exercises have estimated the impact of S1 conditions in the water exchange through the Strait of Sicily (Myers et al., 1998), no paleoceanographic reconstructions have been able to identify the potential impact of such changes in the W-Med surface hydrology to date.

In this study, we present a new detailed characterization of past surface hydrography in the western edge of the Sicily channel (W-Sicily) in order to identify potential variations in the water exchange between the two Mediterranean sub-basins through the Sicily channel associated with the S1 formation. For this purpose, we use a sediment core currently located in the main pathway of the Modified Atlantic Surface Water (MAW) toward the Strait of Sicily. This study focuses in the analysis of the surface hydrographic expression in this area associated to the S1, which has been labeled with the ES1 acronym. Changes in

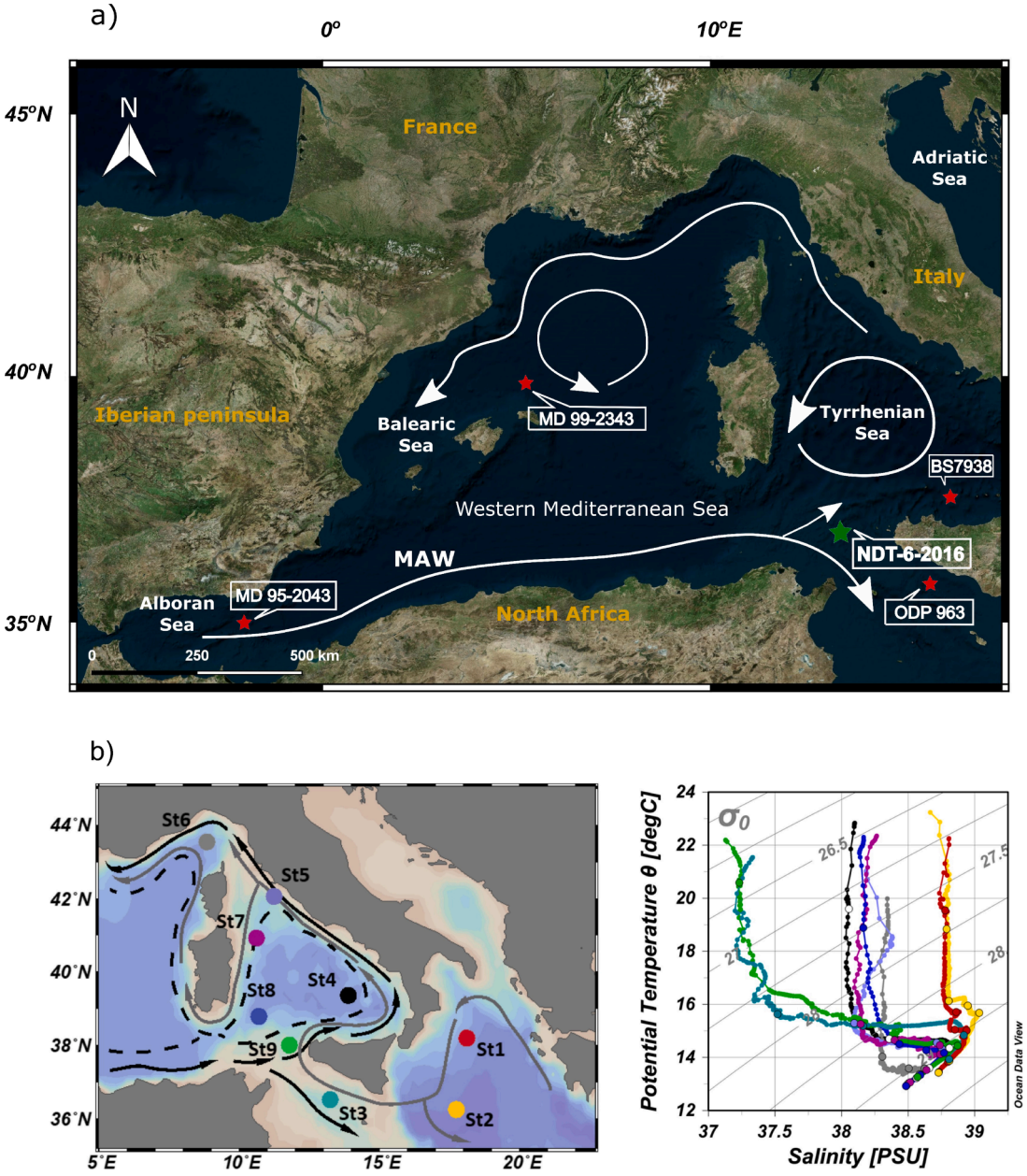

Fig. 1. a) Map of the study area in the western Mediterranean Sea. White arrows represent the Modified Atlantic waters (MAW) and stars represent the cores discussed in this manuscript. Green star represent the studied core NDT-6-2016 and red stars represent the other cores of the western and central Mediterranean Sea. b) Hydrographic stations around the Tyrrhenian Sea, Strait of Sicily and Ionian Sea and its properties in terms of temperature and salinity from Garcia-Solsona et al. (2020), note that location of St9 (green) corresponds to the studied site. (For interpretation of the references to colour in this figure legend, the reader is referred to the web version of this article.)

surface water properties are reconstructed through a multi-proxy approach combining planktic foraminifera ecology, major element analyses in bulk sediments, as well as stable oxygen isotopes measurements ($\delta^{18}O$) in both *Globigerina bulloides* and *Globigerinoides ruber* white variety. The newly generated data are also compared to other available records from the central Mediterranean and the Alboran Sea for further discussion.

2. Materials and methods

2.1. Core description and sampling

The gravity core NDT-6-2016 (~4 m long) was recovered during the Next Data expedition that took place in 2016 on board of CNR-URANIA R/V. The core is located in the transition area between the W-Sicily channel and the southern Tyrrhenian Sea (38°0′26.60" N and 11°47′44.84″E, 1066 m water depth), i.e. at the easternmost region of the W-Med (Fig. 1a). This location is currently sensitive to inter-basin water exchange variability (Fig. 1b) and thus, appropriate to detect potential hydrological changes. Core NDT-6-2016 consists of homogeneous silty-clay sediments with no sedimentary irregularities along the whole sequence. The core was sampled every cm. Planktic foraminifera assemblages were counted every 1–5 cm for the intervals 1–61 cm and 123–340 cm and every 5–20 cm for the rest. Stable isotopes were analysed every 1–2 cm for the interval between 1.20 and 2.60 m (corresponding chronologically to the deglacial-Holocene period) and at lower resolution (5–20 cm) for the rest of the core. Finally, elemental XRF analyses were carried out every cm all along the core.

2.2. Radiocarbon dates and age model

The chronological framework of core NDT-6-2016 was established by twenty ^{14}C dates analysed in monospecific planktic foraminifera samples (>250 μm, *Globorotalia inflata)*. Six ^{14}C ages (Table 1) were measured at The 14Chrono Centre of the Queen's University of Belfast (UK) using a National Electrostatic Corporation (NEC) compact model 0.5MV accelerator mass spectrometer (AMS). Samples were previously treated at the Godwin Laboratory for Palaeoclimate Research of the University of Cambridge (UK), where carbonate shells were turned into graphite following Freeman et al. (2016). Fourteen ^{14}C ages (Table 1) were measured at the ETH Laboratory of Ion Beam Physics (Zurich), using a 200 kV Mini Carbon Dating System (Micadas) with a gas ion source.

Radiocarbon ages were calibrated using MARINE20 calibration curve (Hunt et al., 2020). The age model was constructed using the Bayesian statistics software Bacon (Blaauw and Christeny, 2011) (Table 1). In addition to the ^{14}C dates of the lower part, three tie points were added based on an adjusted alignment between the studied $\delta^{18}O$ record from *G. bulloides* and the well-dated reference NGRIP isotope record (Rasmussen et al., 2006; Vinther et al., 2006). In particular, these selected tie points correlate the onset of the Bølling-Allerød (14.55 kyr BP) and the base and top of the Younger Dryas (YD, 12.89 and 11.57 kyr cal. BP, respectively) (Fig. 2). The sedimentation rates for the studied period (i.e. the last ~15 kyr cal. BP), oscillate between 5.70 and 76.34 cm/kyr, i.e. between 13.10 and 167.56 years per cm (Fig. 2). These results reveal a major decrease in sedimentations rates at around ~10 kyr BP which is validated by a large number of absolute dates supporting that it represents to a major change in the sedimentological processes at the studied location.

2.3. Bulk sediment geochemistry

The analysis of the elemental geochemical composition of core NDT-6-2016 was performed on u-channels sections, with a 10 × 10 mm slit size, and at 1 cm resolution by means of an Avaatech XRF core-scanner at the CORELAB of the Universitat de Barcelona. Excitation conditions were established as follow: a) at 10 kV, 0.5 mA, 10 s with no filter for major elements (Al, Si, S, K, Ca, Ti, Mn and Fe); b) 30 kV, 1 mA, 30 s and Pd-thick filter for heavier elements (mainly Br, Rb, Sr and Zr) and c) 50 kV, 1 mA, 40 s and a Cu filter for Ba. Previous to analysis, u-channels were imaged with a high-resolution line scan camera and covered with a 4 μm SPEXCerti Ultralene foil, which prevents dehydration of the sediment and avoids contamination of the measurement prism.

2.4. Planktic foraminifera taxonomy

Planktic foraminifera species were counted every 2–5 cm for the discussed period (from YD to post-ES1) and between 5 and 20 cm for the rest, from the >125 μm fraction in order to minimise the loss of small species such as *Globigerinita glutinata* o *Turborotalita quinqueloba*

Table 1
^{14}C ages with reservoir age corrections of core NDT-6-2016 and tie points based on the alignment between our stable oxygen isotopes records from *G. bulloides* and stable oxygen isotopes records from well-dated NGRIP (Rasmussen et al., 2006; Vinther et al., 2006). The ages were calibrated using Bayesian statistics software Bacon (Blaauw and Christeny, 2011) and MARINE20 calibration (Hunt et al., 2020).

Depth (cm)	Species	Laboratory	Age ^{14}C (years BP)	2σ error	Calendar (years BP)	Age uncertainties interval (years BP)	Sedimentation rates (cm/kyr)
6	*G. inflata*	ETH Zurich	434	44	103	0–245	
61	*G. inflata*	Godwin Laboratory	3111	28	2972	2798–3148	19.66
83	*G. inflata*	Godwin Laboratory	3718	29	3722	3544–3896	24.83
121	*G. inflata*	ETH Zurich	5319	55	5705	5530–5989	19.45
126	*G. inflata*	Godwin Laboratory	5613	29	6030	5876–6196	19.22
141	*G. inflata*	Godwin Laboratory	6203	28	6659	6483–6835	19.01
151	*G. inflata*	Godwin Laboratory	7432	44	7906	7728–8070	9.08
161	*G. inflata*	Godwin Laboratory	9001	31	9764	9544–9968	6.01
166	*G. inflata*	ETH Zurich	9613	69	10,599	10,291–10,891	14.24
172	*G. inflata*	ETH Zurich	9836	72	10,927	10,665–11,174	26.33
177	*G. inflata*	ETH Zurich	9658	73	10,669	10,393–11,006	37.99
182	*G. inflata*	ETH Zurich	10,000	74	11,151	10,837–11,399	49.02
230	*G. inflata*	ETH Zurich	10,179	73	11,388	11,159–11,690	63.71
242	*G. inflata*	ETH Zurich	9855	71	10,951	10,690–11,186	73.66
255	*G. inflata*	ETH Zurich	9667	73	10,683	10,410–11,018	64.87
259	*G. inflata*	ETH Zurich	11,138	72	12,685	12,489–12,867	56.42
271	Tie point		11,570	200	11,570	11,413–12,113	64.66
286	*G. inflata*	ETH Zurich	11,650	76	13,173	12,960–13,391	56.93
296	*G. inflata*	ETH Zurich	9959	70	11,098	10,792–11,310	71.43
341	Tie point		12,730	200	12,730	12,547–13,323	60.26
360	*G. inflata*	ETH Zurich	11,155	75	12,700	12,498–12,890	52.03
391	*G. inflata*	ETH Zurich	12,513	81	14,227	13,874–14,649	33.98
415	Tie point		14,550	200	14,550	14,394–15,522	34.27

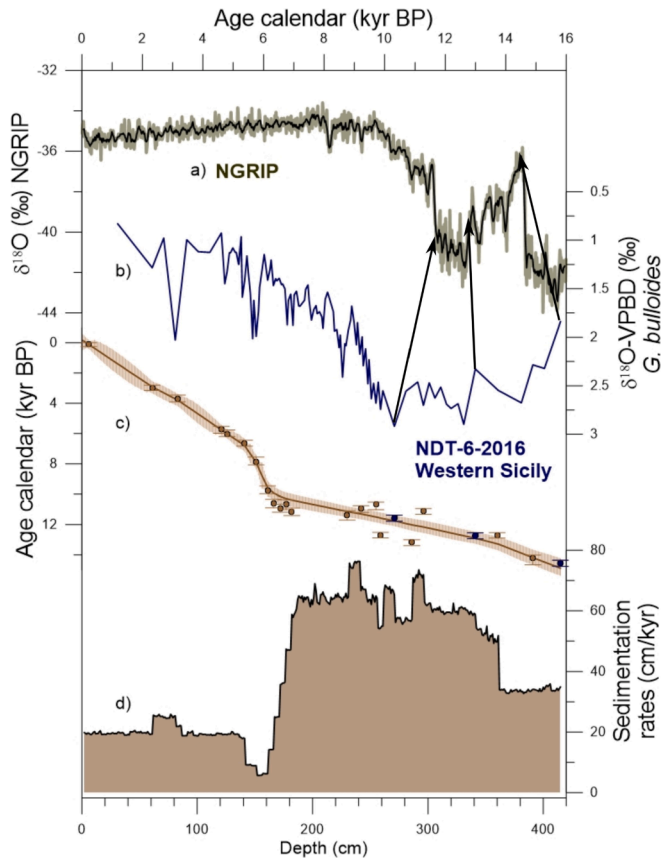

Fig. 2. a) Oxygen isotope record ($\delta^{18}O$) from NGRIP (Rasmussen et al., 2006; Vinther et al., 2006). b) Oxygen isotopes record measured in *G. bulloides* from sediment core NDT-6-2016. c) Age model based on ^{14}C calibrated dates from NDT-6-2016 (represented by brown circles) and three tie points (blue circles) based on the alignment between our *G. bulloides* $\delta^{18}O$ record and stable oxygen isotope record from well-dated NGRIP. d) sedimentation rates of sediment core NDT-6-2016. Note that all records are plotted in the same x axis which represents depth (cm), except the $\delta^{18}O$ record from NGRIP which is plotted in independent x axis representing the Age calendar (kyr BP). (For interpretation of the references to colour in this figure legend, the reader is referred to the web version of this article.)

(Sprovieri et al., 2003). To facilitate the counting, each sample was split between two and four times and a minimum of 300 specimens per sample were counted and normalized to 100. Nineteen groups were distinguished; *Globigerina bulloides* (including *Globigerina falconensis), Globoturborotalita ssp., Globigerinella siphonifera* (including *Globigerinella calida), Globigerinita glutinata, Globigerinoides elongatus, Globigerinoides ruber* white variety, *Globigerinoides ruber* pink variety, *Globigerinoides sacculifer* (including *Globigerinoides trilobus* and *Globigerinoides quadrilobatus*), *Globorotalia inflata, Globorotalia scitula* (dextral and sinistral coiling), *Globorotalia truncatulinoides* (dextral and sinistral coiling), *Neogloboquadrina incompta* (dextral coiling), *Neogloboquadrina pachyderma* (sinistral *coiling), Neogloboquadrina dutertrei, Neogloboquadrina sp., Orbulina universa, Turborotalita quinqueloba* and *Tenuitella spp.*, being *Globigerinita glutinata, Globorotalia inflata, Globigerina bulloides, Turborotalita quinqueloba, Globigerinoides ruber* white variety and *Neogloboquadrina incompta* the most abundant species. The ecological interpretation adopted in this study is based on previous works from Bé & Tolderlund, (1971), Hemleben et al., (1989), Pujol and Vergnaud-Grazzini (1995), Schiebel et al., (2001) and Kucera et al. (2005). Only species with an abundance of >10% of the total assemblages are discussed individually.

2.5. Stable isotopes measurements

Between 10 and 12 specimens of the planktic foraminifera species *G. bulloides* and *G. ruber* white variety were handpicked from the 250–315 μm fraction to analyse the stable oxygen isotopic composition ($\delta^{18}O$) of surface waters. Samples were mechanically cleaned with methanol to remove any attached clay minerals, ultrasonicated for 30 s and dried out under a laminar flood hood. The analyses were conducted using a Finnigan MAT 252 mass spectrometer in the Centre Científic i Tecnològic de la Universitat de Barcelona (CCiT-UB), whose analytical precision for $\delta^{18}O$ is better than 0.08‰. Calibration to Vienna Pee Dee Belemnite (VPDB) was carried out following NBS-19 standards (Coplen, 1996).

3. Results

3.1. Downcore distribution of Planktic foraminifera assemblages

Planktic foraminifera live into the surface waters and are good indicators of climatic conditions since its distribution changes depending on salinity, temperature, vertical water-mixing and surface waters productivity (Bé and Hutson, 1977; Bé and Tolderlund, 1971; Capotondi et al., 1999; Hemleben et al., 1989; Pujol and Vergnaud-Grazzini, 1995; Schiebel and Hemleben, 2000). In this manuscript, we use the distribution of six planktic foraminifera species with different ecological preferences such as *T. quinqueloba, G. glutinata, N. incompta, G. bulloides, G. inflata* and *G. ruber* (Table 2) which allow us to identify four main time intervals (note that the here used ES1 acronym refers to the hydrographic expression of the S1 in the W-Sicily, i.e. changes in the surface hydrology associated to the eastern basin stagnation): 1) the YD (12.95–11.65 kyr cal. BP), characterized by the predominance of *T. quinqueloba* as well as *N. incompta,*; 2) the precedent period to the ES1 (pre-ES1 interval; 11.65–10.5 kyr cal. BP), distinguished by high abundance of both *G. glutinata* and *T. quinqueloba* while *N. incompta* decreased significantly; 3) the ES1 (10.5–7 kyr cal. BP) determined by high presence of *G. inflata* and *G. ruber*; and 4) the post-ES1 (7–6 kyr cal. BP) characterized by high abundance of both *G. inflata* and *N. incompta* and lower values of *G. ruber*. Furthermore, the ES1interval can be divided in two sub-stages: a) the ES1a, characterized by high abundance of *G. inflata* and increasing percentages of *G. ruber* while *T. quinqueloba* and *G. glutinata* tend to decrease and b) the ES1b, distinguished by the highest presence of *G. inflata, N. incompta* and *G. ruber* and the almost total disappearance of *T. quinqueloba* and *G. glutinata*.

Maximum abundance of both *T. quinqueloba* (25–40%) and *G. glutinata* (15–25%) during the YD suggests the prevalence of cold conditions and high-nutrient waters (Fig. 3e and f) (Schmidt et al., 2004). In the modern Mediterranean, both *T. quinqueloba* and *G. glutinata* proliferate during spring as a response to enhanced phytoplankton production, as well as during fall when surface enhanced vertical water column mixing increases and the chlorophyll

Table 2
Summary of planktic foraminifera ecological preferences based on works of (Bé and Tolderlund, 1971), (Hemleben et al., 1989), Pujol and Vergnaud-Grazzini (1995), (Schiebel et al., 2001) and Kucera et al. (2005).

Planktic foraminifera species	Ecological preferences
Turborotalita quinqueloba	Cold and well-mixed high-nutrient waters. Commonly associated with continental run-off.
Globigerinita glutinata	Temperate, well-mixed and high-nutrient waters.
Globigerina bulloides	Cold and temperate waters. High-nutrient and well-mixed waters. Upwelling areas.
Globorotalia inflata	Temperate species. Strong vertical mixing. No Deep chlorophyll maximum (DCM).
Neogloboquadrina incompta	Cold-temperate species. Presence of the DCM.
Globigerinoides ruber	Warm and oligotrophic species. Stratified surface waters.

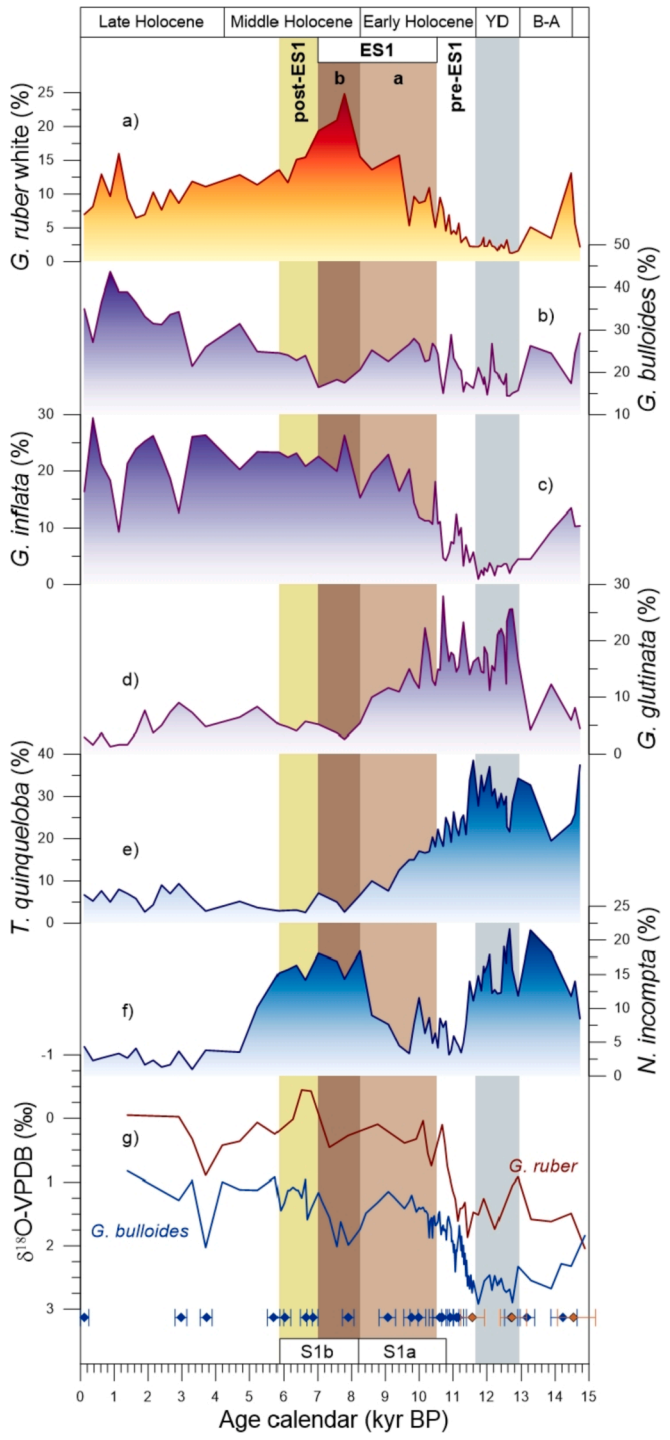

Fig. 3. a-f) Planktic foraminifera distribution and g) $\delta^{18}O$ of planktic foraminifera species *G. bulloides* and *G. ruber* and their ^{14}C calibrated dates with the corresponding errors (blue rhombs) and applied tie points including their uncertainties (orange rhombs). Grey bar represents YD (Younger Dryas), light-brown bar the ES1a, dark-brown bar the ES1b and greenish-yellow bar the post-ES1 (ES1: W-Sicily expression of the S1). (For interpretation of the references to colour in this figure legend, the reader is referred to the web version of this article.)

accumulated during summer in the so-called Deep Chlorophyll Maximum (DCM) is redistributed uniformly in the surface waters (Schiebel et al., 2001). During the same period, the high presence of *N. incompta* (12–20%, Fig. 3f) suggests the presence of a shallow mixed layer and the DCM development, since it proliferated below the thermocline at the end of summer and over fall, when the presence of a shallow nutricline favors the phytoplankton spread (Bé and Hutson, 1977; Pérez-Folgado et al., 2003; Pujol and Vergnaud-Grazzini, 1995; Schiebel et al., 2001). Therefore, during the YD, both *T. quinqueloba* and *G. glutinata* likely predominated during winter/spring when a moderate vertical water-mixing occurred, while *N. incompta* might have prevailed during summer/fall associated with more stratified conditions.

During the pre-ES1 high abundance of both *G. glutinata* (12.5–27.5%) and *T. quinqueloba* (15–25%) (Fig. 3d and e) indicates well-mixed waters and eutrophic conditions (Pujol and Vergnaud-Grazzini, 1995; Sprovieri et al., 2003) as during the YD. But the sharp decrease of *N. incompta* during this period probably indicates a moderate vertical-mixing from the end of summer, which promote the redistribution of nutrients from the DCM favoring the *G. glutinata* and *T. quinqueloba* spread. At the same time, *G. inflata,* that proliferates as a result of thermocline erosion due to the strong vertical mixing conditions (Pujol and Vergnaud-Grazzini, 1995; Sprovieri et al., 2003), show a relatively low abundances (from ~5 to ~10%) (Fig. 3c). Then, planktonic foraminifera distribution during the pre-ES1 suggests an annual homogeneity of the oceanographic conditions, with a weakly developed seasonality.

The ES1 was characterized by maximum abundance of the subtropical species *G. ruber* (10–25%), characteristic of oligotrophic waters (Bonfardeci et al., 2018; Kucera, 2007; Numberger et al., 2009) (Fig. 3a). *G. ruber* grow preferentially during summer conditions in well stratified surface waters (Pujol and Vergnaud-Grazzini, 1995; Schiebel et al., 2001; Sprovieri et al., 2003). *G. inflata* also reaches its highest abundance during this period (oscillating between 12 and 27%) (Fig. 3c). Thus, the ES1 is distinguished by an increase in seasonality with strong winter water-mixing as high abundances of *G. inflata* suggest and by strong summer stratification as *G. ruber* increase point out. The high presence of *N. incompta* (~15%) during the ES1b (Fig. 3f) may suggest the dominance of rather stratified summer/fall conditions with a shallow mixed layer and a DCM development. A different situation than that developed before, during the ES1a, when strong vertical mixing presumably took place during autumn, redistributing the nutrients accumulated in the DCM and favoring the growth of *G. inflata* instead of *N. incompta*. (Bé and Hutson, 1977; Pérez-Folgado et al., 2003; Pujol and Vergnaud-Grazzini, 1995; Schiebel et al., 2001).

During the post-ES1 predominated both *G. inflata* (~22%) and *N. incompta* (~15%) in parallel with a decrease of *G. ruber* (from 20 to 12%) (Fig. 3c and f). While *G. ruber* decrease suggests lower summer-water stratification, *N. incompta* indicates reduced vertical water-mixing and the development of a DCM during fall. During winter, vertical water-mixing would strongly increase as suggested by the high abundance of *G. inflata*.

3.2. Oxygen isotopic records ($\delta^{18}O$)

Oxygen isotopic records ($\delta^{18}O$) from *G. bulloides* and *G. ruber* (Fig. 3g) show a general transition from heavier (glacial) to lighter (interglacial) isotopic values, consistent with the overall global warming and ice sheet melting associated with the last deglaciation (Cacho et al., 2001; Frigola et al., 2007; Rohling et al., 1998; Sbaffi et al., 2004). From ~15 to ~11.7 kyr cal. BP, $\delta^{18}O$ of *G. bulloides* presents a general transition from lighter (~2‰) to heavier values (~3‰). During the YD, heaviest values were dominant ranging between 2.5 and 3‰. Along the pre-ES1 a progressive lightening of 1.5‰ took place (Fig. 3g). During the first part of the ES1 interval (ES1a) $\delta^{18}O$ of *G. bulloides* oscillated between 1 and 1.5‰, while the second part (ES1b) was characterized by a remarkable $\delta^{18}O$ enrichment (~1‰). From the end of the ES1b, $\delta^{18}O$ progressively returned to lighter values. In the case of the *G. ruber* $\delta^{18}O$ record, the evolution was very similar to that of *G. bulloides* but with lighter values (1–2‰), which is consistent with the habitat differences of the two planktic foraminifera; *G. ruber* register the signal of warm and stratified waters, while *G. bulloides* record the signal of colder and mixed

waters. The heaviest *G. ruber* $\delta^{18}O$ values were registered between 15 and 11 kyr cal. BP oscillating between 2 and 1.2‰ (except for the onset of the YD where 1‰ was reached). The pre-ES1 was characterized by a progressive lightening of ~2‰. Along the ES1, $\delta^{18}O$ values were rather constant oscillating between 0 and 0.5‰, while during the post-ES1 a significant depletion took place (from 0.4 to −0.4‰). In general terms, it is remarkable that the overall $\delta^{18}O$ gradient between the two planktic species reached its maximum values during the ES1b interval and the minimum along the pre-ES1 (Fig. 3g).

3.3. Elemental analyses

Profiles of Ti/Al and K/Al ratios present very similar trends throughout the studied interval. These ratios are usually interpreted as indicators of the arrival of terrestrial source material likely reflecting increased sediment supply by river runoff (Frigola et al., 2008; Wehausen and Brumsack, 1998, 2000; Wu et al., 2016). Both ratios reached their maximum values during the pre-ES1 while the ES1 is represented by a relative minimum (Fig. 4a–b). Ba/Ti ratios are often used as an indicator of export primary productivity, since the deposition of barite is associate with primary productivity, although Ba can also have some detrital sources (Martínez-Ruiz et al., 2003; Murray et al., 2000; Paytan and Griffith, 2007). In the case of core NDT-6-2016, the maximum values of Ba/Ti are also reached during the pre-ES1 showing a similar evolution to the previously described ratios (Fig. 4c). During the ES1, however, the Ba/Ti evolution is very distinctive to that of the other ratios, supporting its interpretation in terms of export productivity. In this regard, Ba/Ti ratios present relatively high values during the early ES1 to progressively decrease along that period. From the end of the ES1 to the rest of the record, a general decreasing trend is observed (Fig. 4c). It is interesting to note that the relatively low values in the Ti/Al and K/Al ratios during the ES1 coincides with a major reduction in the sedimentation rates of the NDT-6-2016 core (Fig. 4e), pointing to a decrease in the arrival of detrital source sedimentary particles as a potential cause of these sedimentary changes.

4. Discussion

4.1. Deglacial-Holocene evolution of surface oceanography in W-Sicily

The overall evolution of $\delta^{18}O$ records is consistent with the described deglacial warming trend in the W-Mediterranean (Budillon et al., 2009;

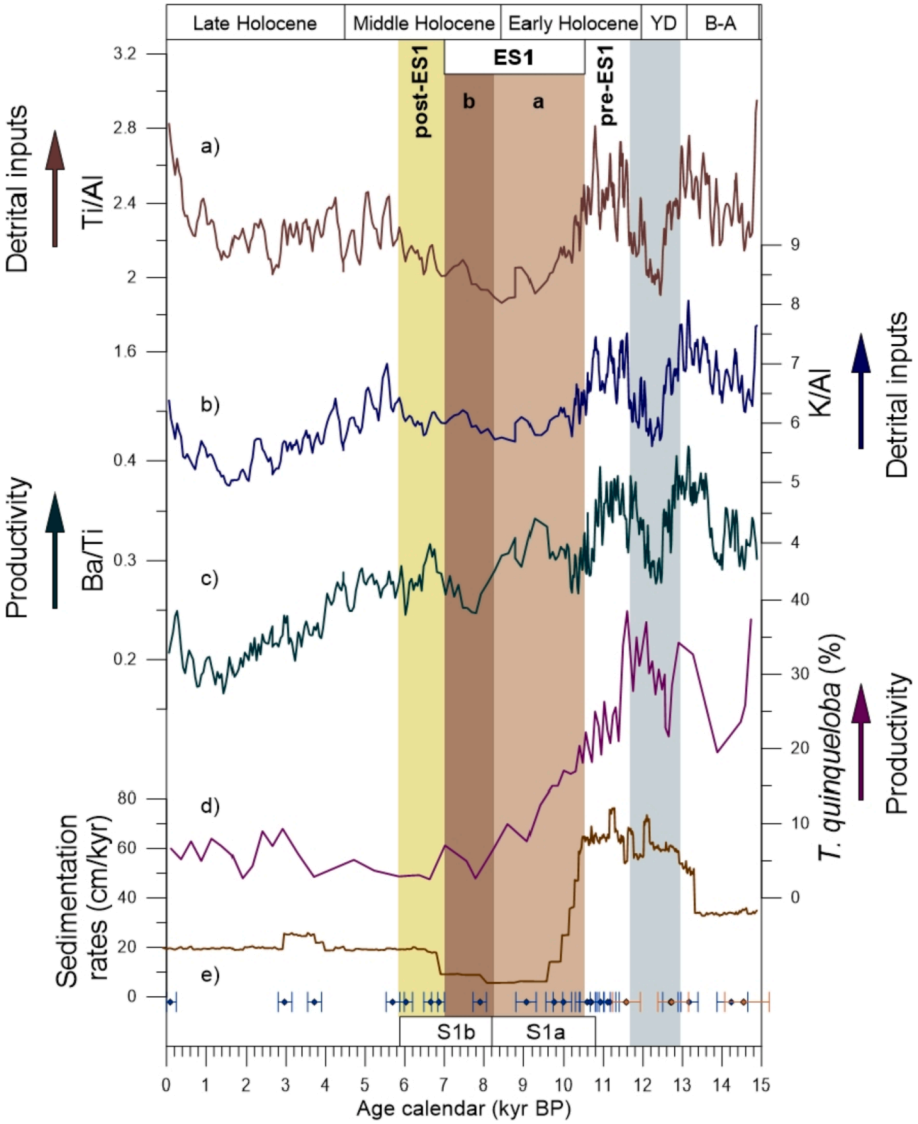

Fig. 4. a-c) Major and minor elements distribution, d) planktic foraminifera distribution of *T. quinqueloba* and e) sedimentation rates of sediment core NDT-6-2016. Blue rhombs represent ^{14}C calibrated dates and orange rhombs represent tie points. Grey bar represents YD, light-brown bar the ES1a, dark-brown bar the ES1b and greenish-yellow bar the post-ES1. (For interpretation of the references to colour in this figure legend, the reader is referred to the web version of this article.)

Cacho et al., 2001; Català et al., 2019; Kallel et al., 1997; Sbaffi et al., 2001). Nevertheless, one of the outstanding findings in our studied core is the distinctive characteristics of the ES1 period (between ~10.5 and ~ 7 kyr cal. BP) in comparison to those developed before (pre-ES1 and YD) and after it.

The predominant high values of both Ti/Al and K/Al ratios during the pre-ES1 (Fig. 4a–b) indicate the arrival of detrital particles to the core location likely due to enhanced continental runoff (Frigola et al., 2008; Wehausen and Brumsack, 2000; Wu et al., 2016). The parallel evolution in Ba/Ti profiles (Fig. 4c) could reflect a relatively high biological productivity (Martínez-Ruiz et al., 2003; Paytan and Griffith, 2007) probably related to the increase in river discharge and the consequent nutrient increase. This interpretation is consistent with a high abundance of planktic foraminifera species with a strong affinity for nutrient-rich surface waters such as *T. quinqueloba* (Fig. 4d) (Margaritelli et al., 2016; Schiebel et al., 2001; Sprovieri et al., 2003). The described high arrival of the detrital particles could be related to the strong African Monsoon activity that started at around 15 kyr BP (Ménot et al., 2020). The general north African humid conditions were interrupted during the YD (Ménot et al., 2020), probably causing the relative minimum in our both Ti/Al and K/Al ratios during this period (Fig. 4a–b). Our core location is currently far from the direct influence of any major river system, but this situation might have been very different during the pre-ES1 coincident with the African humid period, when currently fossil river systems along the North Africa coast were active (Wu et al., 2016, 2017). Considering the local oceanography, detrital particles and nutrients transported by these rivers could reach the studied location through the outflowing intermediate waters from the Strait of Sicily. During the pre–ES1, summer stratification and winter vertical mixing should have been weak according to the low presence of both *G. ruber* and *G. inflata* (Kucera, 2007; Pujol and Vergnaud-Grazzini, 1995). This data, along with the lowest $\delta^{18}O$ gradient between *G. bulloides* and *G. ruber,* support a rather annual homogeneity with a weakly developed seasonality (Fig. 5) since such species represent winter-spring and summer conditions, respectively. Thus, similar values of $\delta^{18}O$ should involve similar conditions across an entire year.

Both bulk sediment chemistry and surface hydrography at the NDT-6-2016 location in the W-Sicily strongly changed at the onset of the ES1. Both Ti/Al and K/Al ratios show minimum values during the whole interval (Fig. 4a–b) while the African humid conditions and associated sediment delivery by the north African river system prevailed (Ménot et al., 2020; Wu et al., 2016). The major reduction in the arrival of detrital source particles is in good agreement with the large reduction of the sediment rates during the whole ES1 (Fig. 4e). However, since this sedimentary change cannot be explained by reduced river runoff, we suggest that it might reflect a major change in the deep water hydrology, likely related to reduction of water exchange through the Strait of Sicily. Consistently, the parallel increment during the ES1 of both *G. inflata*, that predominate with strong water-mixing (typically during winter), and *G. ruber*, that prefer strong surface water stratification conditions (typically during summer), supports the development of a strong seasonality (Fig. 3a,c and Fig. 5) (Hemleben et al., 1989; Pujol and Vergnaud-Grazzini, 1995). This stronger seasonality reached its maxim expression during the ES1b accordingly to the maximum *G. ruber* percentages and it is further supported by the maximum $\delta^{18}O$ gradient between *G. ruber* and *G. bulloides* records (Fig. 3g). The *G. bulloides* $\delta^{18}O$ enrichment observed during the ES1b could reflect the development of extreme winter vertical water-mixing and colder SST (Fig. 7). In contrast, *G. ruber* $\delta^{18}O$ record represented stratified (low nutrient) summer conditions and warmer Sea Surface Temperatures (SST) (Fig. 5). During the post-ES1, a significant decrease in *G. ruber* points to a decrease in surface water stratification during summer, while the high presence of both *N. incompta* and *G. inflata* suggest, on the one hand, relatively stratified conditions with the presence of the DCM during fall and, on the other hand, an intense water-mixing during winter. During the rest of the Holocene period, after post-ES1, a progressive increase in *G. bulloides* parallel with a gradual decrease in *G. ruber* and a sharp decline in *N. incompta* suggests that surface water stratification progressively decreased during summer while more intense water-mixing took place during fall and winter. Furthermore, the sedimentation rates are higher after the ES1, although not as high as during the pre-ES1 (Fig. 4e). These changes in both sedimentary conditions and surface

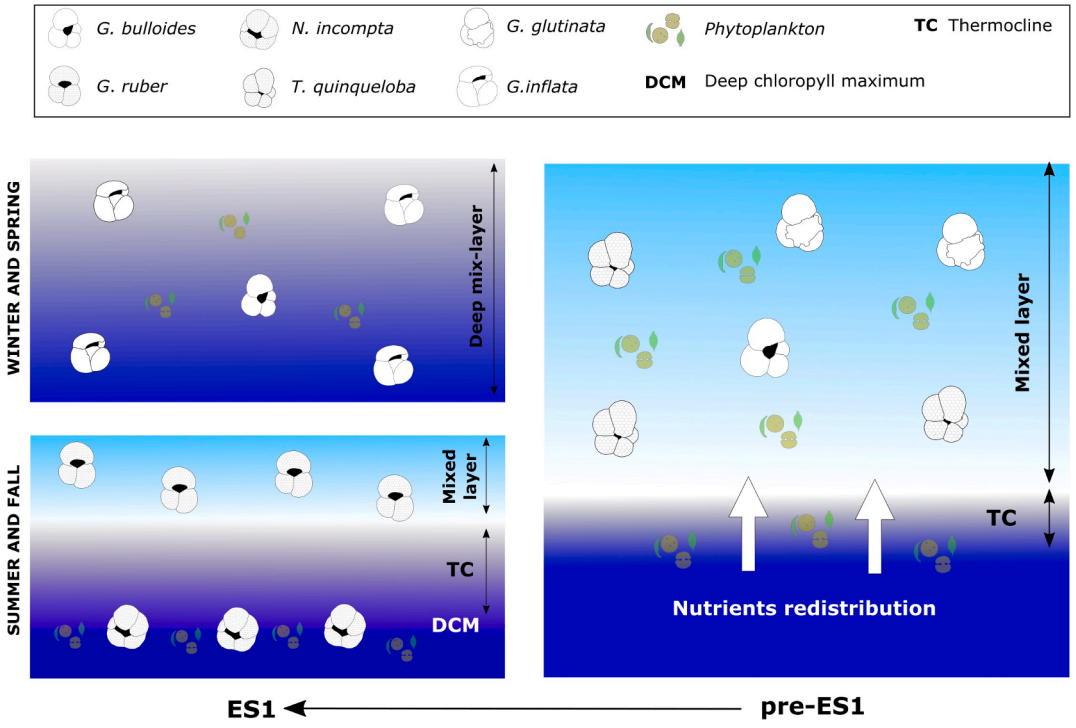

Fig. 5. Scheme representing the planktic foraminifera distribution in the W-Sicily (core NDT-6-2016) during the pre-ES1 and the ES1. Figure represents only the main species dominating each period. It must be noted that changes in planktic foraminifera distribution between periods were progressive.

hydrography were probably related to the end of the extreme stagnation in the *E*-Med and might reflect the arrival of detrital material transported by intermediate waters through the Strait of Sicily, although it was never as high as that during the African humid period that preceded the S1 stagnation.

4.2. Implications of the E-Med S1 stagnation in the central Mediterranean surface oceanography

Our results from W-Sicily during the last ~15 kyr cal. BP can be framed in a broader regional context by comparing our planktic foraminifera results with previously published records from the Alboran Sea (Pérez-Folgado et al., 2003), the southern Tyrrhenian Sea (Sbaffi et al., 2004) and the Strait of Sicily (Sprovieri et al., 2003). We also compare the *G. bulloides* $\delta^{18}O$ records from the same locations (Fig. 7), with the exception of the Sicily channel where no isotopic records are available, and also with an additional record from the Balearic Sea (Català et al., 2019; Frigola et al., 2007).

Oceanographic surface conditions during the YD appear to be rather homogeneous along the considered locations with weak summer stratification conditions (low abundance of *G. ruber*) and weak surface winter water-mixing (low abundance of *G. inflata*). With the onset of the Holocene period (pre-ES1) the surface hydrology conditions begin to differ within the compared locations according to the planktic foraminifera distributions (Fig. 6). In the Strait of Sicily and the southern Tyrrhenian Sea an increased seasonality developed with stronger winter water-mixing conditions (an increase of *G. inflata*) and greater summer water-stratification (an increase of *G. ruber*) (Sbaffi et al., 2004; Sprovieri et al., 2003). In contrast, these species remained relatively low in the Alboran Sea and W-Sicily, probably suggesting the commune influence of the eastward path of the surface Atlantic Waters (MAW). This oceanographic situation would be comparable to that currently observed in the region (Fig. 1b) (Garcia-Solsona et al., 2020), where the station located in in the W-Sicily shows the direct influence of the eastward flow of the surface MAW while the southern Tyrrhenian Sea records a more modified signal in terms of salinity.

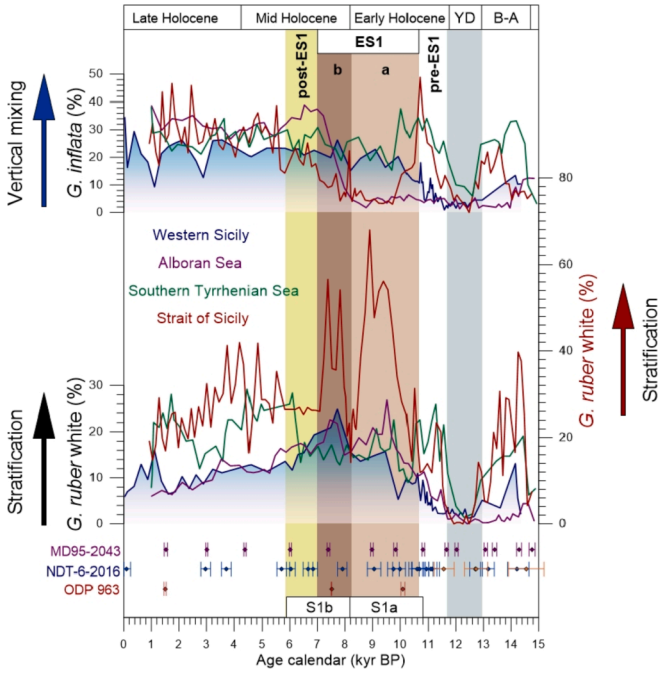

Fig. 6. Planktic foraminifera distribution in the western and central Mediterranean from the studied core NDT-6-2016 and cores BS7938 (Sbaffi et al., 2004), MD95–2043 (Pérez-Folgado et al., 2003) and ODP963 (Sprovieri et al., 2003). Blue line is for the NDT-6-2016, green line for the BS-7938, violet line for MD95–2043 and red line for the ODP963. It must be noted that *G. ruber* distribution from core ODP963 is plotted in independent *y* axis in order to help the figure compression. The ^{14}C calibrated dates used for each chronology are colored accordingly to the corresponding record. In the sediment core NDT-6-2016, blue rhombs represent ^{14}C calibrated dates and orange rhombs represent tie points. Grey bar represents YD, light-brown bar the ES1a, dark-brown bar the ES1b and greenish-yellow bar the post-ES1. (For interpretation of the references to colour in this figure legend, the reader is referred to the web version of this article.)

During the ES1 interval, significant differences are observed between the Strait of Sicily and our W-Sicily location (Fig. 6). Stratified conditions along the whole year predominated in the Strait of Sicily, as the high abundance of *G. ruber* and low presence of *G. inflata* suggests, while a marked seasonality with winter water-mixing and summer stratification, (high *G. inflata* and *G. ruber* abundance) dominated in W-Sicily (Hemleben et al., 1989; Kucera, 2007; Pujol and Vergnaud-Grazzini, 1995). Therefore, hydrographic conditions in W-Sicily resembled more to those already developed in the southern Tyrrhenian Sea during the pre-ES1 and become very distinctive to those in the Alboran Sea (Fig. 6). The comparison of the $\delta^{18}O$ records also supports the distinctive conditions between the W-Sicily and the Alboran Sea with closer similitudes to the southern Tyrrhenian Sea location where both of them (W-Sicily and southern Tyrrhenian Sea) registered a significant $\delta^{18}O$ enrichment (Fig. 7).

In consequence, this site comparison highlights the singular character of the W-Sicily oceanographic conditions during the ES1 and, to some extent, during the pre-ES1. During the YD and after the ES1 the data agree in indicating a good surface interconnection between the W and *E*-Mediterranean basins, letting the W-Sicily and Strait of Sicily locations under the direct influence of the eastern path of the surface Modified Atlantic Waters (MAW). This would be a comparable oceanographic situation to that of the present day (Fig. 1b). During the ES1 a major oceanographic reorganization occurred at the W-Sicily location that we attribute to a restricted sea surface interconnection between the E-Med and the W-Med. While the sea surface conditions in the Sicily channel are coherent with strong annual stratification, likely reflecting the freshening promoted by the African monsoon (Mercone et al., 2001; Rohling et al., 2015; Tachikawa et al., 2015; Tesi et al., 2017), the surface conditions in the W-Sicily were closer to those in the southern Tyrrhenian Sea, probably reflecting the major influence of the predominant climatic conditions in central Europe (Davis et al., 2003; Walker, 1995). This change in the sea surface interconnection between the W-E Med during the ES1 might be a response to the reduced exit of E-Med waters masses through the Strait of Sicily as a consequence of the reduced deep convection in the E-Med (Cornuault et al., 2018; Vadsaria et al., 2019; Wu et al., 2019). This would agree with the observed major reduction in the detrital particles transport toward the studied site detected by the Ti/Al and K/Al ratios and sedimentation rates (Fig. 4a–b, e). Although our data cannot provide any direct insight into the intermediate and deep circulation, the parallel changes in sea surface condition and in sedimentary patterns support a tided link between them, which is consistent with a major weakening in the Strait of Sicily exchange at both surface and deep layers.

5. Summary and conclusions

Our new data from sediment core NDT-6-2016 in the W-Sicily allow the characterization of very distinctive oceanographic conditions during the ES1 interval (10.5–7 kyr cal. BP), as compared to the pre-ES1 and post-ES1. During the pre-ES1 interval, the W-Sicily records reflect low seasonality that progressively increased at the onset of the ES1 with summer stratification and winter mixing. These conditions turned more extreme during the ES1b and changed progressively along the post-ES1 toward lower seasonality. A comparison of our $\delta^{18}O$ and planktic foraminifera distribution results, with similar records from the Alboran Sea, Balearic Sea, Tyrrhenian Sea and Strait of Sicily reveals that the ES1 conditions in our location contrasted to those developed in the Sicily

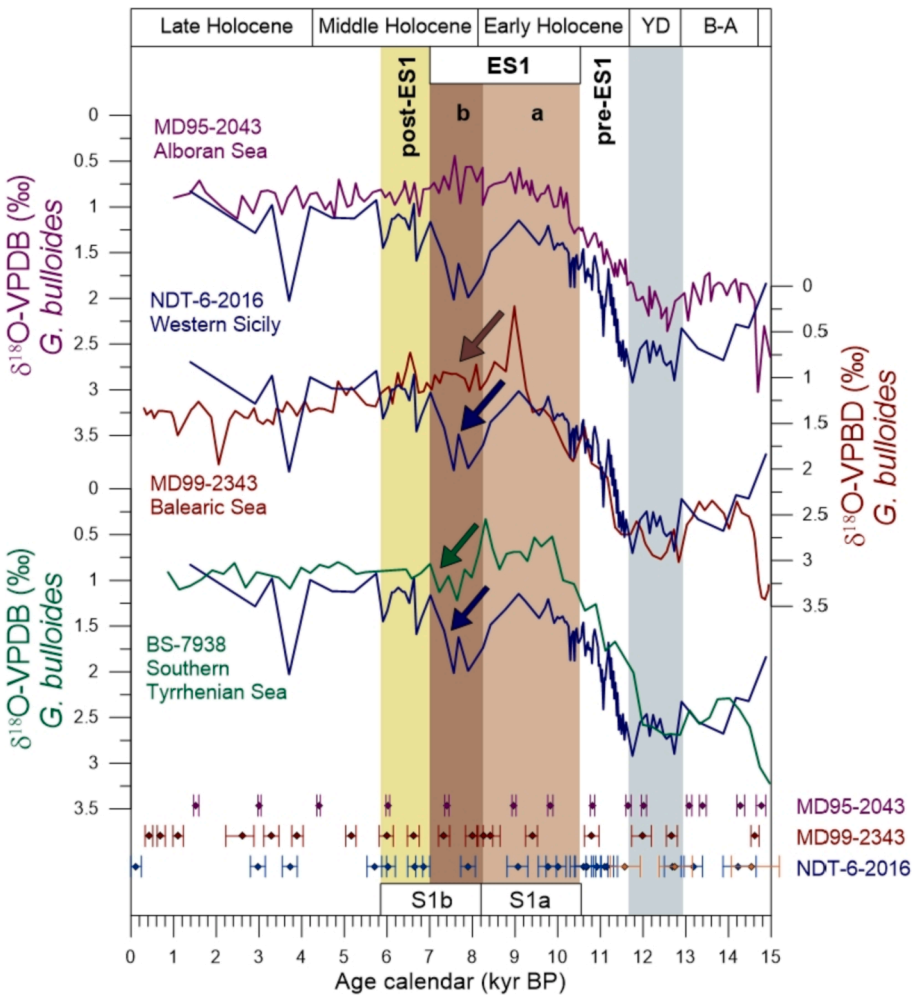

Fig. 7. Comparison of $\delta^{18}O$ (VPDB) records from different locations of the western Mediterranean Sea throughout the last 15 kyr cal. BP and chronological control for individual records. Blue line represents the $\delta^{18}O$ record from the studied core NDT-6-2016. From the top to the base in violet, red and green colour $\delta^{18}O$ records from the cores MD95–2043 (Cacho et a., 1999), MD99–22343 (Frigola et al., 2007; Català et al., 2019) and BS-7938 (Sbaffi et al., 2004) respectively. The ^{14}C calibrated dates used for each chronology are colored accordingly to the corresponding record. For core NDT-6-2016, blue rhombs represent ^{14}C calibrated dates and orange rhombs represent tie points. Grey bar represents YD, light-brown bar the ES1a, dark-brown bar the ES1b and greenish-yellow bar the post-ES1. (For interpretation of the references to colour in this figure legend, the reader is referred to the web version of this article.)

channel and also in the Alboran Sea, showing higher similarity to those of the Tyrrhenian Sea. This is an opposite situation to that developed during YD when conditions in W-Sicily were closer to those of the Sicily channel and the Alboran Sea, a situation coherent with the current oceanography at these locations directly affected by the eastern path of the MAW. Consequently, we propose that during the ES1 a reduced surface water interconnection between E-Med and W-Med prevailed likely driven by the E-Med stagnation. This oceanographic condition resulted in a reduced thermohaline circulation that caused a weakening of the eastward flow of Atlantic source surface waters, reducing its entrance through the Strait of Sicily and over the studied W-Sicily site. In consequence, the predominant conditions that prevailed in central-southern Europe during the ES1 interval played an essential role, promoting the observed high seasonality in the W-Sicily oceanographic conditions. Therefore, our data provide a solid support for a major surface oceanographic reorganization in the central Mediterranean associated with the S1 formation in the Eastern Mediterranean Sea.

Declaration of Competing Interest

The authors declare that they have no known competing financial interests or personal relationships that could have appeared to influence the work reported in this paper.

Acknowledgements

This work was founded by the projects TIMED (683237) of the European Research Council (Consolidator Grants) and NextData PNR 2011–2013 (http://www.nextdataproject.it/). The GRC Geociències Marines thank the Generalitat de Catalunya for the Grups de Recerca Consolidats grant 2017 SGR 315. Leopoldo D. Pena acknowledges support from the Ramón y Cajal program (MINECO, Spain), Isabel Cacho from the ICREA Academia programme from the Generalitat de Catalunya, Jaime Frigola from the Serra Húnter Programme (Generalitat de Catalunya). We thank the doctoral school in Earth and Sea Sciences from University of Palermo which supported the research. We also thank ISMAR-CNR (Napoli) for core NDT-6-2016 which it was recovered by the NEXTDATA expedition on board R/V CNR-Urania in 2014. We acknowledge Montse Guart (Dept. Dinàmica de la Terra i de l'Oceà, Universitat de Barcelona) and Joaquim Perona (Centres Científics i Tecnològics, CCiT-UB) for their support with the laboratory work. Finally, we thank the editor and the anonymous reviewers for their comments, which substantially improved this manuscript.

References

Abrantes, F., Voelker, A., Sierro, F.J., Naughton, F., Rodrigues, T., Cacho, I., Ariztegui, D., Brayshaw, D., Sicre, M.A., Batista, L., 2012. Paleoclimate variability in the mediterranean region. In: The Climate of the Mediterranean Region, First Edit. Elsevier Inc. https://doi.org/10.1016/B978-0-12-416042-2.00001-X.

Bé, A.W.H., Hutson, W.H., 1977. Ecology of Planktonic Foraminifera and Biogeographic patterns of Life and Fossil Assemblages in the Indian Ocean. Micropaleontology 23 (4), 369. https://doi.org/10.2307/1485406.

Bé, A.W.H., Tolderlund, D.S., 1971. Distribution and ecology of living planktonic foraminifera in surface waters of the Atlantic and Indian oceans. Micropalaentol. Oceans 105–149.

Bethoux, J.P., 1993. Mediterranean sapropel formation, dynamic and climatic viewpoints. Oceanol. Acta 16 (2), 127–133.

Bianchi, D., Zavatarelli, M., Pinardi, N., Capozzi, R., Capotondi, L., Corselli, C., Masina, S., 2006. Simulations of ecosystem response during the sapropel S1 deposition event. Palaeogeogr. Palaeoclimatol. Palaeoecol. 235 (1–3), 265–287. https://doi.org/10.1016/j.palaeo.2005.09.032.

Blaauw, M., Christeny, J.A., 2011. Flexible paleoclimate age-depth models using an autoregressive gamma process. Bayesian Anal. 6 (3), 457–474. https://doi.org/10.1214/11-BA618.

Bonfardeci, A., Caruso, A., Bartolini, A., Bassinot, F., Blanc-Valleron, M.M., 2018. Distribution and ecology of the Globigerinoides ruber — Globigerinoides elongatus morphotypes in the Azores region during the late Pleistocene-Holocene. Palaeogeogr. Palaeoclimatol. Palaeoecol. 491 (November), 92–111. https://doi.org/10.1016/j.palaeo.2017.11.052.

Budillon, F., Lirer, F., Iorio, M., Macrì, P., Sagnotti, L., Vallefuoco, M., Ferraro, L., Garziglia, S., Innangi, S., Sahabi, M., Tonielli, R., 2009. Integrated stratigraphic reconstruction for the last 80 kyr in a deep sector of the Sardinia Channel (Western Mediterranean). Deep-Sea Res. Part II: Topical Stud. Oceanogr. 56 (11–12), 725–737. https://doi.org/10.1016/j.dsr2.2008.07.026.

Cacho, I., Grimalt, J.O., Canals, M., Sbaffi, L., Shackleton, N., Schönfeld, J., Zahn, R., 2001. Variability of the western Mediterranean Sea surface temperature during the last 25,000 years and its connection with the northern hemisphere climatic changes. Clim. Chang. 16 (1), 40–52. https://doi.org/10.1029/sp010.

Capotondi, L., Maria Borsetti, A., Morigi, C., 1999. Foraminiferal ecozones, a high resolution proxy for the late Quaternary biochronology in the Central Mediterranean Sea. Mar. Geol. 153 (1–4), 253–274. https://doi.org/10.1016/S0025-3227(98)00079-6.

Català, A., Cacho, I., Frigola, J., Pena, L.D., Lirer, F., 2019. Holocene hydrography evolution in the Alboran Sea: a multi-record and multi-proxy comparison. Clim. Past 15 (3), 927–942. https://doi.org/10.5194/cp-15-927-2019.

Checa, H., Margaritelli, G., Pena, L.D., Frigola, J., Cacho, I., Rettori, R., Lirer, F., 2020. High resolution paleo-environmental changes during the Sapropel 1 in the North Ionian Sea, Central Mediterranean. Holocene. https://doi.org/10.1177/0959683620941095.

Coplen, Tyler B., 1996. New guidelines for reporting stable hydrogen, carbon, and oxygen isotope-ratio data. Geochim. Cosmochim. Ac. 60, 3359–3360. https://doi.org/10.1016/0016-7037(96)00263-3 (17).

Cornuault, M., Tachikawa, K., Vidal, L., Guihou, A., Siani, G., Deschamps, P., Bassinot, F., Revel, M., 2018. Circulation changes in the Eastern Mediterranean Sea over the past 23,000 years Inferred from Authigenic Nd Isotopic Ratios. Paleoceanogr. Paleoclimatol. 33 (3), 264–280. https://doi.org/10.1002/2017PA003227.

Davis, B.A.S., Brewer, S., Stevenson, A.C., Guiot, J., Allen, J., Almqvist-Jacobson, H., Ammann, B., Andreev, A.A., Argant, J., Atanassova, J., Balwierz, Z., Barnosky, C.D., Bartley, D.D., De Beaulieu, J.L., Beckett, S.C., Behre, K.E., Bennett, K.D., Berglund, B. E.B., Beug, H.J., Zernitskaya, V.P., 2003. The temperature of Europe during the Holocene reconstructed from pollen data. Quat. Sci. Rev. 22 (15–17), 1701–1716. https://doi.org/10.1016/S0277-3791(03)00173-2.

De Lange, G.J., Thomson, J., Reitz, A., Slomp, C.P., Speranza Principato, M., Erba, E., Corselli, C., 2008. Synchronous basin-wide formation and redox-controlled preservation of a Mediterranean sapropel. Nat. Geosci. 1 (9), 606–610. https://doi.org/10.1038/ngeo283.

Filippidi, A., Triantaphyllou, M.V., De Lange, G.J., 2016. Eastern-Mediterranean ventilation variability during sapropel S1 formation, evaluated at two sites influenced by deep-water formation from Adriatic and Aegean Seas. Quat. Sci. Rev. 144, 95–106. https://doi.org/10.1016/j.quascirev.2016.05.024.

Freeman, E., Skinner, L.C., Reimer, R., Scrivner, A., Fallon, S., 2016. Graphitization of small carbonate samples for paleoceanographic research at the Godwin radiocarbon laboratory, University of Cambridge. Radiocarbon 58 (1), 89–97. https://doi.org/10.1017/RDC.2015.8.

Frigola, J., Moreno, A., Cacho, I., Canals, M., Sierro, F.J., Flores, J.A., Grimalt, J.O., Hodell, D.A., Curtis, J.H., 2007. Holocene climate variability in the western Mediterranean region from a Deepwater sediment record. Paleoceanography 22 (2), 1–16. https://doi.org/10.1029/2006PA001307.

Frigola, J., Moreno, A., Cacho, I., Canals, M., Sierro, F.J., Flores, J.A., Grimalt, J.O., 2008. Evidence of abrupt changes in Western Mediterranean Deep Water circulation during the last 50 kyr: a high-resolution marine record from the Balearic Sea. Quat. Int. 181 (1), 88–104. https://doi.org/10.1016/j.quaint.2007.06.016.

Garcia-Solsona, E., Pena, L.D., Paredes, E., Pérez-Asensio, J.N., Quirós-Collazos, L., Lirer, F., Cacho, I., 2020. Rare earth elements and Nd isotopes as tracers of modern ocean circulation in the Central Mediterranean Sea. Prog. Oceanogr. 185 (December 2019), 102340. https://doi.org/10.1016/j.pocean.2020.102340.

Grant, K.M., Grimm, R., Mikolajewicz, U., Marino, G., Ziegler, M., Rohling, E.J., 2016. The timing of Mediterranean sapropel deposition relative to insolation, sea-level and African monsoon changes. Quat. Sci. Rev. 140, 125–141. https://doi.org/10.1016/j.quascirev.2016.03.026.

Grimm, R., Maier-reimer, E., Mikolajewicz, U., Schmiedl, G., Mu, K., Adloff, F., Grant, K. M., Ziegler, M., Lourens, L.J., Emeis, K., 2015. Late Glacial Initiation of Holocene Eastern Mediterranean Sapropel Formation. https://doi.org/10.1038/ncomms8099.

Hemleben, C., Spindler, M., Anderson, O.R., 1989. Modern Planktonic Foraminifera. Springer-Verlag. https://doi.org/10.1017/CBO9781107415324.004.

Hunt, Chris O., Farrell, Michelle, Katrin, Fenech, et al., 2020. Chronology and stratigraphy of the valley systems. Temple landscapes Fragility, change and resilience of Holocene environments in the Maltese Islands, 1. McDonald Institute for Archaeological Research, Cambridge, UK, pp. 35–71.

Incarbona, A., Sprovieri, M., Lirer, F., Sprovieri, R., 2011. Surface and deep water conditions in the Sicily channel (Central Mediterranean) at the time of sapropel S5 deposition. Palaeogeogr. Palaeoclimatol. Palaeoecol. 306 (3–4), 243–248. https://doi.org/10.1016/j.palaeo.2011.04.030.

Kallel, N., Paterne, M., Labeyrie, L., Duplessy, J.C., Arnold, M., 1997. Temperature and salinity records of the Tyrrhenian Sea during the last 18,000 years. Palaeogeogr. Palaeoclimatol. Palaeoecol. 135 (1–4), 97–108. https://doi.org/10.1016/S0031-0182(97)00021-7.

Kucera, M., 2007. Chapter six planktonic foraminifera as tracers of past oceanic environments. Dev. Marine Geol. 1 (07), 213–262. https://doi.org/10.1016/S1572-5480(07)01011-1.

Kucera, M., Weinelt, M., Kiefer, T., Pflaumann, U., Hayes, A., Weinelt, M., Te Chen, M., Mix, A.C., Barrows, T.T., Cortijo, E., Duprat, J., Juggins, S., Waelbroeck, C., 2005. Reconstruction of sea-surface temperatures from assemblages of planktonic foraminifera: Multi-technique approach based on geographically constrained calibration data sets and its application to glacial Atlantic and Pacific Oceans. Quat. Sci. Rev. 24 (7–9 SPEC. ISS), 951–998. https://doi.org/10.1016/j.quascirev.2004.07.014.

Lourens, L.J., Hilgen, F.J., Gudjonsson, L., Zachariasse, W.J., 1992. Late Pliocene to early Pleistocene astronomically forced sea surface productivity and temperature variations in the Mediterranean. Mar. Micropaleontol. 19 (1–2), 49–78. https://doi.org/10.1016/0377-8398(92)90021-B.

Margaritelli, G., Vallefuoco, M., Di Rita, F., Capotondi, L., Bellucci, L.G., Insinga, D.D., Petrosino, P., Bonomo, S., Cacho, I., Cascella, A., Ferraro, L., Florindo, F., Lubritto, C., Lurcock, P.C., Magri, D., Pelosi, N., Rettori, R., Lirer, F., 2016. Marine response to climate changes during the last five millennia in the Central Mediterranean Sea. Glob. Planet. Chang. 142, 53–72. https://doi.org/10.1016/j.gloplacha.2016.04.007.

Marino, G., Rohling, E.J., Sangiorgi, F., Hayes, A., Casford, J.L., Lotter, A.F., Kucera, M., Brinkhuis, H., 2009. Early and middle Holocene in the Aegean Sea: interplay between high and low latitude climate variability. Quat. Sci. Rev. 28 (27–28), 3246–3262. https://doi.org/10.1016/j.quascirev.2009.08.011.

Martínez-Ruiz, F., Paytan, A., Kastner, M., González-Donoso, J.M., Linares, D., Bernasconi, S.M., Jimenez-Espejo, F.J., 2003. A comparative study of the geochemical and mineralogical characteristics of the S1 sapropel in the western and eastern Mediterranean. Palaeogeogr. Palaeoclimatol. Palaeoecol. 190, 23–37. https://doi.org/10.1016/S0031-0182(02)00597-7.

Mayewski, P.A., Rohling, E.J., Stager, J.C., Karlén, W., Maasch, K.A., Meeker, L.D., Meyerson, E.A., Gasse, F., van Kreveld, S., Holmgren, K., Lee-Thorp, J., Rosqvist, G., Rack, F., Staubwasser, M., Schneider, R.R., Steig, E.J., 2004. Holocene climate variability. Quat. Res. 62 (3), 243–255. https://doi.org/10.1016/j.yqres.2004.07.001.

Ménot, G., Pivot, S., Bouloubassi, I., Davtian, N., Hennekam, R., Bosch, D., Ducassou, E., Bard, E., Migeon, S., Revel, M., 2020. Timing and stepwise transitions of the African Humid Period from geochemical proxies in the Nile deep-sea fan sediments. Quat. Sci. Rev. 228 https://doi.org/10.1016/j.quascirev.2019.106071.

Mercone, D., Thomson, J., Abu-Zied, R.H., Croudace, I.W., Rohling, E.J., 2001. High-resolution geochemical and micropalaeontological profiling of the most recent eastern Mediterranean sapropel. Mar. Geol. 177 (1–2), 25–44. https://doi.org/10.1016/S0025-3227(01)00122-0.

Murat, A., 1999. Pliocene – Pleistocene occurrence of sapropels in the western Mediterranean Sea and their relation to eastern Mediterranean sapropels. In: Proceedings of the Ocean Drilling Program, Scientific Results, 161, pp. 519–527.

Murray, R.W., Knowlton, C., Leinen, M., Mix, A.C., Polsky, C.H., 2000. Export production and carbonate dissolution in the central equatorial Pacific Ocean over the past 1 Myr. Paleoceanography 15 (6), 570–592. https://doi.org/10.1029/1999PA000457.

Myers, P.G., Haines, K., Rohling, E.J., 1998. Modeling the paleocirculation of the Mediterranean: the last glacial maximum and the Holocene with emphasis on the formation of sapropel S1. Paleoceanography 13 (6), 586–606. https://doi.org/10.1029/98PA02736.

Numberger, L., Hemleben, C., Hoffmann, R., Mackensen, A., Schulz, H., Wunderlich, J. M., Kucera, M., 2009. Habitats, abundance patterns and isotopic signals of morphotypes of the planktonic foraminifer Globigerinoides ruber (d'Orbigny) in the eastern Mediterranean Sea since the Marine Isotopic Stage 12. Mar. Micropaleontol. 73 (1–2), 90–104. https://doi.org/10.1016/j.marmicro.2009.07.004.

Paytan, A., Griffith, E.M., 2007. Marine barite: recorder of variations in ocean export productivity. Deep-Sea Res. Part II: Topical Stud. Oceanogr. 54 (5–7), 687–705. https://doi.org/10.1016/j.dsr2.2007.01.007.

Pérez-Folgado, M., Sierro, F.J., Flores, J.A., Cacho, I., Grimalt, J.O., Zahn, R., Shackleton, N., 2003. Western Mediterranean planktonic foraminifera events and millennial climatic variability during the last 70 kyr. Mar. Micropaleontol. 48 (1–2), 49–70. https://doi.org/10.1016/S0377-8398(02)00160-3.

Pujol, C., Vergnaud-Grazzini, C., 1995. Distribution patterns of live planktic foraminifers as related to regional hydrography and productive systems of the Mediterranean Sea. Mar. Micropaleontol. 25 (2–3), 187–217. https://doi.org/10.1016/0377-8398(95)00002-I.

Rasmussen, S.O., Andersen, K.K., Svensson, A.M., Steffensen, J.P., Vinther, B.M., Clausen, H.B., Johnsen, S.J., Larsen, L.B., Bigler, M., Ro, R., Fischer, H., 2006. A new Greenland Ice Core Chronology for the Last Glacial Termination, 111, pp. 1–16. https://doi.org/10.1029/2005JD006079.

Rohling, E.J., 1994. Review and new aspects concerning the formation of eastern Mediterranean sapropels. Mar. Geol. 122 (1–2), 1–28. https://doi.org/10.1016/0025-3227(94)90202-X.

Rohling, E.J., Hayes, A., De Rijk, S., Kroon, D., Zachariasse, W.J., Eisma, D., 1998. Abrupt cold spells in the Northwest Mediterranean. Paleoceanography 13 (4), 316–322. https://doi.org/10.1029/98PA00671.

Rohling, E.J., Marino, G., Grant, K.M., 2015. Mediterranean climate and oceanography, and the periodic development of anoxic events (sapropels). Earth Sci. Rev. 143, 62–97. https://doi.org/10.1016/j.earscirev.2015.01.008.

Rossignol-Strick, M., 1985. Mediterranean Quaternary sapropels, an immediate response of the African monsoon to variation of insolation. Palaeogeogr. Palaeoclimatol. Palaeoecol. 49 (3–4), 237–263. https://doi.org/10.1016/0031-0182(85)90056-2.

Sbaffi, L., Wezel, F.C., Kallel, N., Paterne, M., Cacho, I., Ziveri, P., Shackleton, N., 2001. Response of the pelagic environment to palaeoclimatic changes in the Central Mediterranean Sea during the late Quaternary. Mar. Geol. 178 (1–4), 39–62. https://doi.org/10.1016/S0025-3227(01)00185-2.

Sbaffi, L., Wezel, F.C., Curzi, G., Zoppi, U., 2004. Millennial- to centennial-scale palaeoclimatic variations during termination I and the Holocene in the Central Mediterranean Sea. Glob. Planet. Chang. 40 (1–2), 201–217. https://doi.org/10.1016/S0921-8181(03)00111-5.

Schiebel, R., Hemleben, C., 2000. Interannual variability of planktic foraminiferal populations and test flux in the eastern North Atlantic Ocean (JGOFS). Deep-Sea Res. Part II: Topical Stud. Oceanogr. 47 (9–11), 1809–1852. https://doi.org/10.1016/S0967-0645(00)00008-4.

Schiebel, R., Waniek, J., Bork, M., Hemleben, C., 2001. Planktic foraminiferal production stimulated by chlorophyll redistribution and entrainment of nutrients. Deep-Sea Res. Part I: Oceanogr. Res. Papers 48 (3), 721–740. https://doi.org/10.1016/S0967-0637(00)00065-0.

Schmidt, D.N., Renaud, S., Bollmann, J., Schiebel, R., Thierstein, H.R., 2004. Size distribution of Holocene planktic foraminifer assemblages: Biogeography, ecology and adaptation. Mar. Micropaleontol. 50 (3–4), 319–338. https://doi.org/10.1016/S0377-8398(03)00098-7.

Sprovieri, R., Di Stefano, E., Incarbona, A., Gargano, M.E., 2003. A high-resolution record of the last deglaciation in the Sicily Channel based on foraminifera and calcareous nannofossil quantitative distribution. Palaeogeogr. Palaeoclimatol. Palaeoecol. 202 (1–2), 119–142. https://doi.org/10.1016/S0031-0182(03)00632-1.

Tachikawa, K., Vidal, L., Cornuault, M., Garcia, M., Pothin, A., Sonzogni, C., Bard, E., Menot, G., Revel, M., 2015. Eastern Mediterranean Sea circulation inferred from the conditions of S1 sapropel deposition. Clim. Past 11 (6), 855–867. https://doi.org/10.5194/cp-11-855-2015.

Tesi, T., Asioli, A., Minisini, D., Maselli, V., Dalla Valle, G., Gamberi, F., Langone, L., Cattaneo, A., Montagna, P., Trincardi, F., 2017. Large-scale response of the Eastern Mediterranean thermohaline circulation to African monsoon intensification during sapropel S1 formation. Quat. Sci. Rev. 159, 139–154. https://doi.org/10.1016/j.quascirev.2017.01.020.

Toucanne, S., Angue Minto'o, C.M., Fontanier, C., Bassetti, M.A., Jorry, S.J., Jouet, G., 2015. Tracking rainfall in the northern Mediterranean borderlands during sapropel deposition. Quat. Sci. Rev. 129, 178–195. https://doi.org/10.1016/j.quascirev.2015.10.016.

Vadsaria, T., Ramstein, G., Dutay, J.C., Li, L., Ayache, M., Richon, C., 2019. Simulating the occurrence of the last sapropel event (S1): Mediterranean basin ocean dynamics simulations using Nd isotopic composition modeling. Paleoceanogr. Paleoclimatol. 34 (2), 237–251. https://doi.org/10.1029/2019PA003566.

Vinther, B.M., Clausen, H.B., Johnsen, S.J., Rasmussen, S.O., Andersen, K.K., Buchardt, S. L., Seierstad, I.K., Steffensen, J.P., Svensson, A., Olsen, J., Heinemeier, J., 2006. A Synchronized Dating of Three Greenland Ice Cores throughout the Holocene, 111, pp. 1–11. https://doi.org/10.1029/2005JD006921.

Walker, M.J.C., 1995. Climatic changes in Europe during the last glacial/interglacial transition. Quat. Int. 28 (C), 63–76. https://doi.org/10.1016/1040-6182(95)00030-M.

Wehausen, R., Brumsack, H.J., 1998. The formation of Pliocene Mediterranean sapropels: Constraints from high-resolution major and minor element studies. In: Proceedings of the Ocean Drilling Program: Scientific Results, 160, pp. 207–218. https://doi.org/10.2973/odp.proc.sr.160.004.1998.

Wehausen, R., Brumsack, H.J., 2000. Chemical cycles in Pliocene sapropel-bearing and sapropel-barren eastern Mediterranean sediments. Palaeogeogr. Palaeoclimatol. Palaeoecol. 158 (3–4), 325–352. https://doi.org/10.1016/S0031-0182(00)00057-2.

Wu, J., Böning, P., Pahnke, K., Tachikawa, K., de Lange, G.J., 2016. Unraveling North-African riverine and eolian contributions to Central Mediterranean sediments during Holocene sapropel S1 formation. Quat. Sci. Rev. 152, 31–48. https://doi.org/10.1016/j.quascirev.2016.09.029.

Wu, J., Liu, Z., Stuut, J.B.W., Zhao, Y., Schirone, A., de Lange, G.J., 2017. North-African paleodrainage discharges to the Central Mediterranean during the last 18,000 years: a multiproxy characterization. Quat. Sci. Rev. 163 (May), 95–113. https://doi.org/10.1016/j.quascirev.2017.03.015.

Wu, J., Pahnke, K., Böning, P., Wu, L., Michard, A., de Lange, G.J., 2019. Divergent Mediterranean seawater circulation during Holocene sapropel formation – Reconstructed using Nd isotopes in fish debris and foraminifera. Earth Planet. Sci. Lett. 511, 141–153. https://doi.org/10.1016/j.epsl.2019.01.036.